A Letters Journal Exploring the Frontiers of Physics

September 2014

EPL, **107** (2014) 64002
doi: 10.1209/0295-5075/107/64002

www.epljournal.org

# Evaporative microclimate driven hygrometers and hygromotors

Jun Young Chung[1,2], Hunter King[1] and L. Mahadevan[1,2,3(a)]

[1] *School of Engineering and Applied Sciences, Harvard University - Cambridge, MA 02138, USA*
[2] *Wyss Institute for Biologically Inspired Engineering, Harvard University - Cambridge, MA 02138, USA*
[3] *Department of Physics, Harvard University - Cambridge, MA 02138, USA*

received 18 July 2014; accepted in final form 25 August 2014
published online 15 September 2014

PACS 46.70.De – Beams, plates, and shells
PACS 68.03.Fg – Evaporation and condensation of liquids

**Abstract** – A strip of paper placed on a hand spontaneously curls upwards. This simple observation illustrates the ability of a relatively homogeneous hygroscopic structural material, paper, to sense and respond to the microclimate near a non-equilibrium system, a moist evaporative boundary layer. We quantify this interaction using a simple experiment and show that it can be understood in terms of a minimal model. A small modification of this paper hygrometer that makes one or another surface partly hydrophobic using a crayon or tape allows us to create a hygro-oscillator or a hygromotor that converts transverse moisture gradients into lateral oscillations or directed motion. Our study shows how treating paper as a responsive structural material allows us to extract information and work from a microclimatic boundary layer, transforming a messenger to a machine.



The ability to effectively measure an environmental parameter or actuate a device relies on a large, reversible response to a small external stimulus. Sensors often utilize the disproportionate trade-off between small mechanical response and large change in electrical properties, such as in the case of piezoelectric and capacitive sensors. In order to obtain reversible, large mechanical response, ancient strategies in biology and recent advances in engineering have utilized soft materials, such as in the actuation of natural and synthetic muscles [1–3]. A complementary theme in mechanoreception can be found in diverse biological situations involving slender objects which allow small varying lateral strains to cause large changes in shape *via* bending. Indeed natural examples include the opening/closing of pine cones [4] and curling of wheat awns [5] and have also inspired artificial analogs for potential engineering applications [3,6–8].

A natural candidate for a responsive slender structure that might serve as a hygromorphic sensor or actuator is paper, a fibrous porous sheet of cellulose fibers that is inexpensive, versatile, and sustainable. As a disordered material, paper derives its rigidity from entanglement and adhesion of its composite fibers. The athermal and frictional nature of its relatively large fibers (length $\approx 1\,\mathrm{mm}$, diameter $\approx 10\,\mu\mathrm{m}$) fundamentally distinguishes its response [9,10] from otherwise analogous thermal polymeric solids; indeed the relation to these solids is similar to that between jammed granular systems and molecular glasses. During the fabrication of paper, the alignment of fibers along the direction of deposition by fluid leads to a marked mechanical anisotropy [9]. This, together with the fact that cohesion between composite cellulose fibrils is mediated by inter- and intra-molecular hydrogen bonds sensitive to stimuli such as humidity, heat, solvent concentration, and ionic strength [11–13], means that varying these parameters leads to expansion or contraction of the network, preferentially in the direction perpendicular to the alignment direction. Though typical strains may be small, strain gradients across the thickness can lead to large out-of-plane deflections.

Figure 1(a) shows how a thin sheet of paper placed on one's palm curls as it swells on one side in response to the exudation of moisture from the skin. When skin is replaced by a moist sponge from which water evaporates at a controlled rate, we observe a similar phenomenon (see the appendix for experimental details). In fig. 1(b), (c), we show two small pieces of paper, a lightweight yellow paper and a heavyweight white paper, placed on the sponge spontaneously curl and bend upward from their edges. Both papers preferentially bend perpendicular to the fiber alignment, the effect being more pronounced in the heavier paper, which has greater fiber alignment

(a) E-mail: lm@seas.harvard.edu

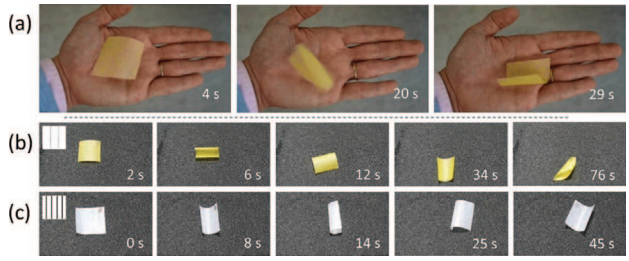


Fig. 1: (Color online) Curling, rolling, and flipping of paper on moist surfaces. (a) Curling of paper on a human palm (see also the supplementary video, `Movie1.mov`). (b), (c): snapshots showing the random curling of two different kinds of commercial papers deposited on a moist sponge: tracing paper with a relatively weak fiber orientation (b); weighing paper with a strong unidirectional fiber orientation (c) (see also the supplementary video, `Movie2.mov`). The insets in the first snapshot of (b) and (c) show the direction of predominant fiber orientation.

(see the appendix). Eventually the paper curls over so strongly that it tips over its edge and flips upside down, exposing the drier side to moisture, and the process repeats itself. This reproducible, reversible nature is in marked contrast to the irreversible curling of paper that occurs on a water surface [14,15] but similar to that observed in engineered polymer films that can harvest energy from humidity [3,8].

The bending is due to the moisture-driven differential expansion of paper, which depends on the relative humidity difference across its thickness, with $H_1 - H_2 > 0$, where the subscripts 1 and 2 refer, respectively, to the bottom (close to the moist surface) and top sides of the paper. The local humidity gradient near a moist surface is the result of both vapor diffusion and advection into an infinite bath, non-equilibrium processes which can depend strongly on the local flow patterns, the geometry of the surface, and ambient relative humidity (*e.g.*, see ref. [16]). Such local "microclimates", like that which creates the humidity difference $\Delta H$ across the paper, have been observed near ($\lesssim 3\,\mathrm{cm}$) living tissues, such as a transpiring leaf [17]. In our setting, assuming the paper to be approximately uniform through the thickness $h$ (along the $\tilde{z}$-axis), the steady-state humidity gradient across the paper will be roughly linear:

$$H(\tilde{z}) = H_1 - \frac{\Delta H}{h}\tilde{z}, \tag{1}$$

where $\Delta H = H_1 - H_2$. In the range $20\% < H < 65\%$, paper is known to reversibly and linearly absorb water vapor and expand with strain $\epsilon$ with a material-dependent, hygroscopic expansion coefficient $\alpha$ [11]:

$$\epsilon = \alpha H. \tag{2}$$

Then, the gradient in strain caused by differential expansion leads to the sheet bending with a curvature $\kappa$ given by

$$\kappa = \frac{\mathrm{d}\epsilon}{\mathrm{d}\tilde{z}} = \frac{\alpha}{h}\Delta H. \tag{3}$$

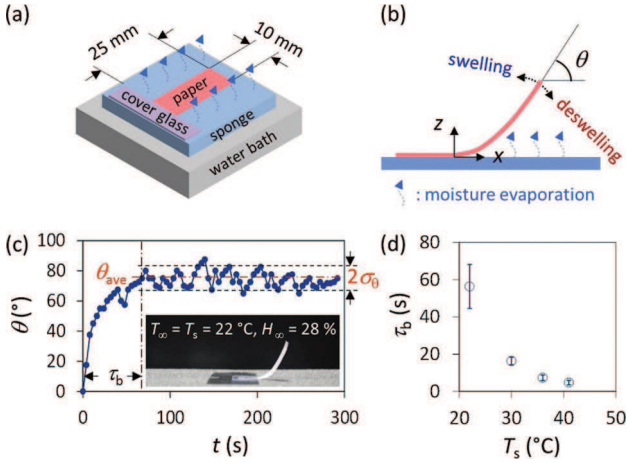


Fig. 2: (Color online) The bending of a paper cantilever deposited on a moist sponge. (a) Schematic of the experimental setup. (b) Schematic side view indicating the bending angle $\theta$. (c) Measured $\theta$ as a function of time $t$ in an open-air environment with an ambient temperature $T_\infty$ of [22.4±0.2] °C and relative humidity $H_\infty$ of [28.3±1.4]% (see also the supplementary video, `Movie3.mov`). The inset shows a representative photograph for $\theta_{ave} \approx 74°$. (d) Curling time scale $\tau_b$ as a function of surface temperature $T_s$ (at $T_\infty \approx 22\,^\circ\mathrm{C}$ and $H_\infty \approx 28\%$). The error bars represent the standard deviation for three samples prepared under identical conditions.

This result is similar to those of bilayer systems [6,18], where strains caused by incompatible expansion through the thickness lead to curvature. By contrast, the linear strain gradient in this case allows for a stress-free solution, in which elastic moduli play no role.

To test this model, we employ a simple cantilever geometry (fig. 2(a), (b)), where an initially flat paper rests on the surface of a moist sponge at time $t = 0$ with one edge ($x = 0$, $z = 0$) permanently clamped. Gradually, the free end bends upward making an angle $\theta$ with the horizontal, eventually reaching an average value $\theta_{ave}$ in a characteristic time $\tau_b$ of about 60 s (for typical lab conditions) and then fluctuating around it with a deviation $\sigma_\theta$, as shown in fig. 2(c). This characteristic time is associated with the time for the moisture to diffusively move through the fibers and void spaces in the paper, and can be expressed as $\tau_b \simeq h^2/D$, where $D$ is the diffusivity of moisture in paper. Using measured thickness and reported values of $D$ [19], we find that $\tau_b \in [10, 100]\,\mathrm{s}$, which reasonably matches the measured response time (fig. 2(d)).

The curvature of the paper is greatest nearest the surface, decreasing near its free end (see the inset in fig. 2(c)), which fluctuates owing to a varying local humidity associated with the varying microclimate. To characterize this microclimate, we directly measure the relative humidity profile $H(z)$ normal to the surface (without paper) for identical surface preparations, but on days with significantly variable ambient relative humidity $H_\infty$, measured with a small capacitive humidity sensor, as shown in fig. 3(a). (That the relative humidity does not reach 100%

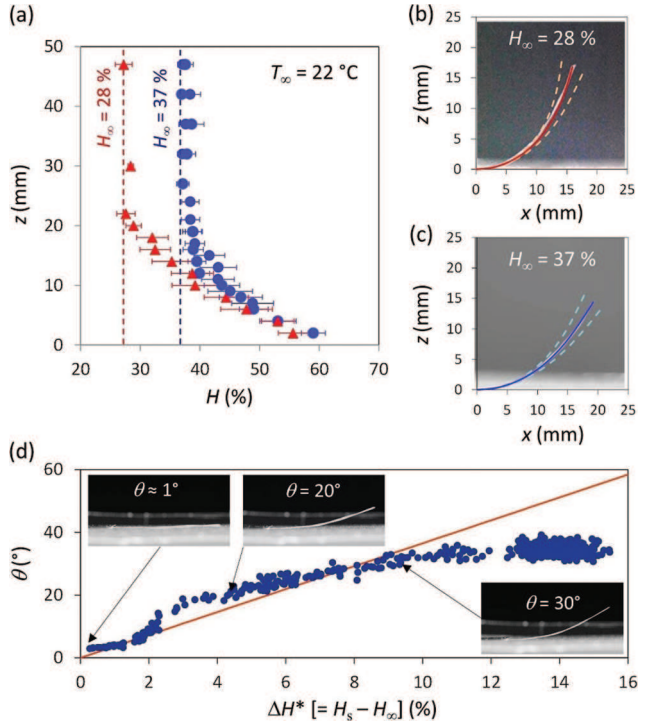


Fig. 3: (Color online) (a) Profiles of the relative humidity $H$ measured along the vertical axis $z$ for two different values of $H_\infty$. The error bars represent the standard deviation $\sigma_H$ of the fluctuations around the mean $H_{ave}$. (b), (c): shape comparison between the experiments (background photographs are instances of the tip angle $\theta = \theta_{ave}$) and theoretical predictions (solid curves: mean; dashed curves: deviation) for: $H_\infty = [28.3\pm1.4]\%$ ($T_\infty = [22.4\pm0.2]\,^\circ$C) (b) and $H_\infty = [37.3\pm0.8]\%$ ($T_\infty = [21.8\pm0.2]\,^\circ$C) (c). (d) Measured $\theta$ *vs.* the relative humidity difference $\Delta H^*$ between the near surface of a drying sponge $H_s$ and the ambient air $H_\infty$ (at $T_\infty \approx 21\,^\circ$C and $H_\infty \approx 47\%$; initial $H_s \approx 62\%$). The solid line corresponds to the relation $\theta \approx \frac{180L}{\pi}\frac{\alpha}{h}\Delta H^*$ with $L = 25\,$mm, $h = 40\,\mu$m, and $\alpha = 1.02\times10^{-4}$.

at the near surface of a moist sponge is consistent with the fact that its free volume is not saturated with liquid water.) Coincident fluctuations observed in simultaneous measurements at two nearby heights (see the appendix) suggest that much of the variation is due to random fluid motions, despite having a protected setup to minimize ventilating currents.

In predicting the deformed shape of the paper cantilever, we use the local relation, eq. (3), and apply it to the measured average humidity profiles: $\kappa(z) = (\alpha/h)\Delta H(z)$, where $\Delta H(z) \approx [H_{ave}(z) \pm \sigma_H(z)] - H_\infty$ (approximating the paper as impermeable to vapor transport on time scales associated with bending), and $\sigma_H(z)$ is the fluctuating part of the relative humidity. Though the approximation somewhat underestimates both $H_1$, because moisture does accumulate under the paper, and $H_2$, because some moisture is transported to the top, it provides a relatively more accurate estimate of the difference $\Delta H$, which ultimately determines local curvature.

We use the form of the curvature $\kappa(z)$ with a fixed boundary condition at $x = 0$: $z(x = 0) = 0$ and $\mathrm{d}z/\mathrm{d}x(x = 0) = 0$, where $\alpha$ is a free parameter to best fit the image of the cantilever in fig. 3(b), having measured the thickness ($h = 40\,\mu$m). The result yields $\alpha = 1.02\times10^{-4}$, consistent with values in the literature [11,20]. The same value was applied to the predicted curve in fig. 3(c), for which the measured humidity was significantly different. The predicted standard deviation curves, shown in fig. 3(b), (c) by the dashed curves, were generated using the measured values of $\sigma_H(z)$.

The agreement between predicted and measured cantilever shapes for two sets of environmental conditions with one common fitting parameter indicates that, despite the large variation in both measured humidity and bending angle, the average values of each can be meaningfully related to each other through our simple model. That the predicted deviation curves reasonably bound the variation shown in the images (indicated by $\sigma_\theta$ in fig. 2(c)) suggests that the cantilever shape simply follows the change in relative humidity, which is, in turn, sensitive to fluctuations in air flow.

We note that in addition to the dependence on ambient relative humidity and flow conditions, the sensitivity of a paper sensor is also determined by the rate of evaporation, which, in turn, depends on substrate properties such as surface humidity, surface temperature, and salinity (see the appendix). In fig. 3(d), we show the strong dependence of the bending angle of paper $\theta$ on the humidity difference $\Delta H^* = H_s - H_\infty$ over time while the sponge slowly dried out ($H_s$ is the relative humidity measured very near ($\approx 3\,$mm) to the surface of the drying sponge). The solid line represents a crude estimate for $\theta$ in which $\kappa = \text{const} = \frac{\alpha}{h}\Delta H^*$, ignoring the interactive role of paper geometry and humidity profile.

Having seen how a uniform hygroscopic material, paper, can be used as a simple measure of the evaporative microclimate near a moist surface, we now show that it can be used to do mechanical work using the energy harnessed from evaporation. By modifying one or both surfaces to inhibit absorption or expansion, one can build hygro-oscillators and hygromotors as shown in fig. 4. Upon partially coating a strip of paper along two opposite edges with a piece of moisture-resistant tape and depositing it on a moist surface, we see that it first bends upward symmetrically due to the swelling of the paper just below the tape. However, this U-shaped state is not stable and tips over into a C-shape (or its mirror image), that flattens out due to drying, before the whole process is repeated. These rocking side-to-side oscillations have an average period $\tau_p$, the typical time required to bend the sheet into a U starting from a flat sheet (the time to tip over is much smaller than the time to bend the sheet). In typical lab conditions, $\tau_p \approx \tau_b \approx 50\,$s (fig. 4(a)–(c)).

On the other hand, by introducing a glide-flip symmetry, and coating the top of one edge of the paper and the bottom of the opposite edge with a piece of tape,

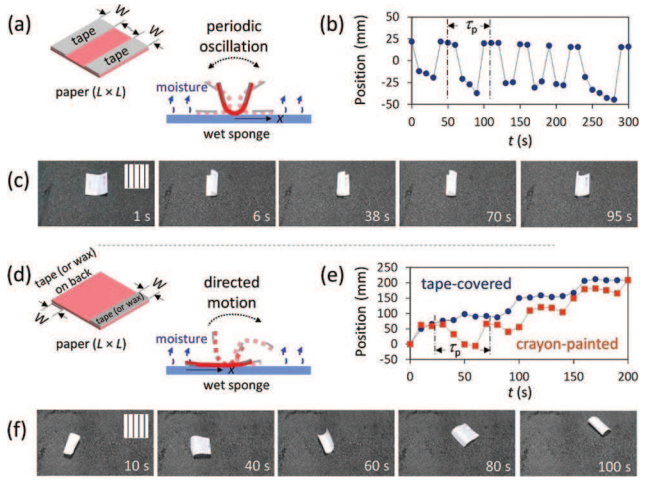


Fig. 4: (Color online) Paper hygro-oscillator and hygromotor. (a)–(c) Periodic, symmetric oscillatory bending motion perpendicular to fiber orientation: schematic of a partially tape-covered paper ($L = 50\,\text{mm}$, $W = 19\,\text{mm}$) on a moist sponge (a); measured $x$ positions of the initial right edge plotted against time for a 10 s time interval (b); Time-lapse snapshots (see also the supplementary video, `Movie4.mov`) (c). (d)–(f) Directed motion by rolling: schematic of a selectively tape-covered ($L = 50\,\text{mm}$, $W = 6\,\text{mm}$) or wax-coated paper ($L = 50\,\text{mm}$, $W = 8\,\text{mm}$) on a moist sponge (d); measured positions of the center point of the initial left edge along a moving path plotted against time for a 10 s interval (e); snapshots for the selectively tape-covered paper, showing directed motion by rolling from left to right (f) (see also the supplementary video, `Movie5.mov`). The insets in the first snapshot of (c) and (f) show the direction of predominant fiber orientation.

we can convert oscillations to directed motion via flipping (fig. 4(d)–(f)). As only one edge of the side of the paper in contact with the moist surface is free to swell, the strip bends over and eventually loses stability as it is shaped into a C (or its mirror image), and flips over. Because of the lack of up-down symmetry, the same process when repeated leads to net motion. The time for flipping once the strip bends strongly is small compared to the time for bending; therefore the period of motion is determined by the time for bending into a C. This leads to discontinuous motor trajectories with a period for flipping $\tau_p \approx 50\,\text{s}$, again, consistent with the time for a paper cantilever to bend in the microclimatic boundary layer (fig. 2(c)), and yields an average velocity determined by the length of the strip, *i.e.*, $\approx 3.5\,\text{cm}/50\,\text{s} = 0.7\,\text{mm s}^{-1}$. This effect can be achieved even more simply by replacing the tape with a thin layer of hydrophobic paraffin wax from a crayon (see fig. 4(d), (e)).

We note that the average period of turnover $\tau_p$ for both types of paper actuators is nearly the same and is comparable to the characteristic time $\tau_b$ needed to reach the quasi-stationary curl in paper (fig. 2(c)). Since the bending dynamics of the paper is strongly regulated by substrate properties (see the appendix), placing a paper actuator onto a moist surface with a higher $T_s$ (see fig. 2(d)) or salinity will cause it to either speed up or slow down. The relative width of the tape patch (or wax painted portion) compared to the half-width of the paper $2W/L$ is another factor that affects motor parameters such as frequency and velocity, although it is not as significant as the humidity variation. There should be an optimal ratio of $2W/L$ for maximizing the motor efficiency, as either limit is poorly behaved: if $2W/L \sim 1$, the paper sheet cannot bend enough to tip or flip over so that it remains relatively stable, while if $2W/L \ll 1$, the asymmetry disappears, leaving the situation in fig. 1(c).

Our results show that the generic heterogeneous swelling response of a piece of paper can be used to extract information and work from the microclimate near a moist surface. In particular, the reproducible variations in both the substrate and the environment allow for cheap hygrosensors, while the symmetry-breaking modifications allow us to power non-equilibrium microclimate-driven hygromotors. A minimal model accurately describes the familiar, though non-trivial mechanics of these devices and is suggestive of the ease with which one might engineer and optimize sensors or devices by manipulating microstructure or macro-geometry.

* * *

We acknowledge support from the Wyss Institute for Biologically Inspired Engineering at Harvard University, the Human Frontiers Science Program, NSF Harvard MRSEC DMR–0820484, and the MacArthur Foundation (LM).

## Appendix

White weighing paper (VWR Scientific Products; basis weight $= 39\,\text{g m}^{-2}$; thickness $\approx 40\,\mu\text{m}$), lightweight yellow tracing paper (Alvin; basis weight $= 31\,\text{g m}^{-2}$; thickness $\approx 30\,\mu\text{m}$), adhesive tape (Scotch Magic Tape, 3M; basis weight $= 65\,\text{g m}^{-2}$; thickness $\approx 50\,\mu\text{m}$), crayon (Crayola), double-sided tape (3M), and cover glass (Cover Glass No. 1 (22 mm × 50 mm), Corning; thickness $\approx 150\,\mu\text{m}$) were purchased from local suppliers. The sponge used in this study was an open cell, polyurethane foam used for packaging to protect products. The sodium chloride (NaCl) was purchased from Sigma-Aldrich and used as received. In the present study, a small piece of the weighing paper was chosen as the main test sample for its highly anisotropic nature exhibiting different mechanical properties in its principal directions due to preferential fiber orientation (see fig. 5).

A porous polymeric foam placed on a water bath (a moist sponge) was used as a controlled evaporative substrate. A piece of porous foam was cut into suitable size and placed in a container made of aluminum foil, which had been partially filled with pure water. Evaporative water loss through the surface of a moist sponge was determined by monitoring the weight change over time, and the result showed that the evaporation rate remained fairly constant (see fig. 6(a)).

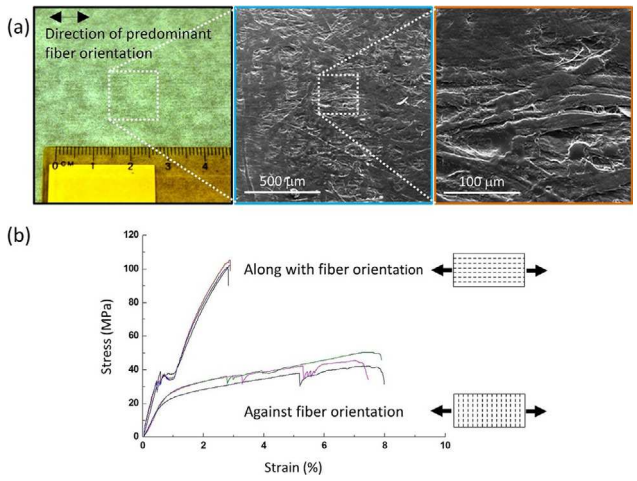


Fig. 5: (Color online) Structural and mechanical properties of the weighing paper. (a) Photograph and scanning electron microscope images. (b) Stress-strain curves obtained from tensile tests (strain rate = 0.8 mm min$^{-1}$) along with fiber orientation (machine direction) and against fiber orientation (cross-machine direction), showing that the paper is highly anisotropic, with a higher modulus ($E$ = [7.20±0.22] GPa) and a higher fracture stress ($\sigma$ = [100.9±3.6] MPa) in the machine direction than in the cross-machine direction ($E$ = [3.83±0.06] GPa and $\sigma$ = [41.7±2.1] MPa, respectively). Different colors correspond to repeated measurements.

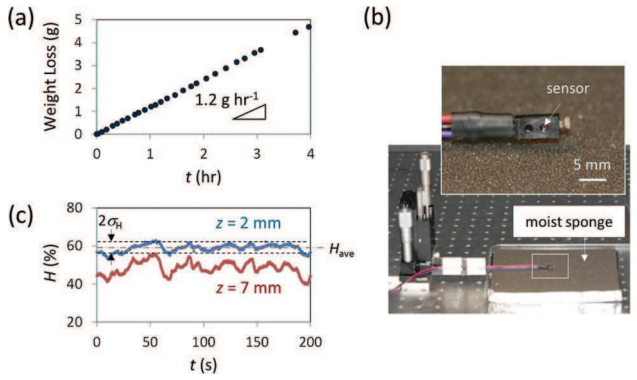


Fig. 6: (Color online) Relative humidity measurements near the surface of a moist sponge. (a) Water loss by evaporation through the surface of a moist sponge (area ≈ 0.025 m$^2$) measured in an open-air environment with an ambient temperature $T_\infty \approx 22\,^\circ$C and an ambient relative humidity $H_\infty \approx 30\%$. The result indicates that the evaporation rate is fairly constant over time and the evaporative flux in this case is $\approx 1.3 \times 10^{-5}$ kg m$^{-2}$ s$^{-1}$. (b) Photograph of the experimental setup used for the relative humidity measurements. (c) Representative measurements of relative humidity $H$ at different heights $z$ obtained by a pair of sensors at $T_\infty \approx 22\,^\circ$C and $H_\infty \approx 37\%$. Comparing these results with those presented in fig. 2(c) suggests that the fluctuation of the bending angle of paper is possibly caused by the fluctuation of the relative humidity.

The temperature $T_\infty$ and relative humidity $H_\infty$ of ambient air and the surface temperature $T_s$ of a moist sponge were measured with a thermo-hygro sensor (Fisher Scientific) and a surface mounted thermocouple, respectively. Movies of the paper motion were taken with a digital camera (Lumix DMC-GF2, Panasonic) equipped with a zoom lens (Lumix G Vario 14-42 mm lens). All the experiments reported in this study were carried out with a small piece of the paper that was deposited on a moist sponge (size = 175 mm × 140 mm, thickness = 15 mm) with pure water (≈ 100 mL) in an open-air laboratory environment with $T_\infty$ = [22±1] °C, $H_\infty$ = [28±1]%, and $T_s$ = [22±1] °C, unless otherwise specified.

The experiments shown in fig. 1(b), (c) were conducted with an about 50 mm square paper deposited on the surface of a moist sponge having a size of 540 mm × 420 mm and a thickness of 25 mm with ≈ 500 mL of pure water.

In the bending experiments shown in figs. 2 and 3, a paper cantilever made of the weighing paper with a length of 25 mm and a width of 10 mm was used. A cantilever-shaped section (35 mm in length, 10 mm in width) was cut out of the sheet of paper, with fiber orientation (*i.e.*, machine direction) perpendicular to the length of the paper. A 10 mm portion of one end in length of the paper cantilever was sandwiched between two cover glasses and secured with a double-stick tape, while the remaining portion was free. The paper cantilever was then gently placed on the surface of a moist sponge, and the bending process was recorded using the digital-camera system. The variations with time of the bending angles at the free end of the curled cantilever were analyzed using the recorded video images. The local curvatures along the curled cantilever were also analyzed and found to exhibit the same trend as the bending angle with time as shown in fig. 2(c). The bending angle was chosen for analysis in the present study due to its ease of accurate measurement as compared to the local curvatures.

In the measurements of the humidity gradient shown in fig. 3(a), a capacitive humidity probe (HIH-4030-003, Honeywell) was used. The probe was mounted on a rigid frame attached to two linear translation stages (Oriel/Newport) allowing for fine adjustments in vertical distance from the surface of a moist sponge up to several centimeters (see fig. 6(b)). The sensing face of the probe was oriented perpendicular to the surface to minimize any possible interference with moisture flow. The probe was manually displaced and positioned above the near center of the surface, and measurements were made along the height axis $z$ (from top to bottom) in about 5 mm steps between 20 mm and 50 mm and in about 2 mm steps below 20 mm. Measurements were performed for several different values of $H_\infty$ at constant $T_\infty$ and, results for two of them were presented in fig. 3(a): $H_\infty$ = [27.7±0.6]% ($T_\infty$ = [21.7±0.1] °C) and $H_\infty$ = [37.3±0.8]% ($T_\infty$ = [21.8±0.2] °C). In one experiment, pairs of sensors whose sensing portions were vertically separated by ≈ 5 mm were used for the simultaneous measurement of relative humidity at two different locations (see fig. 6(c)).

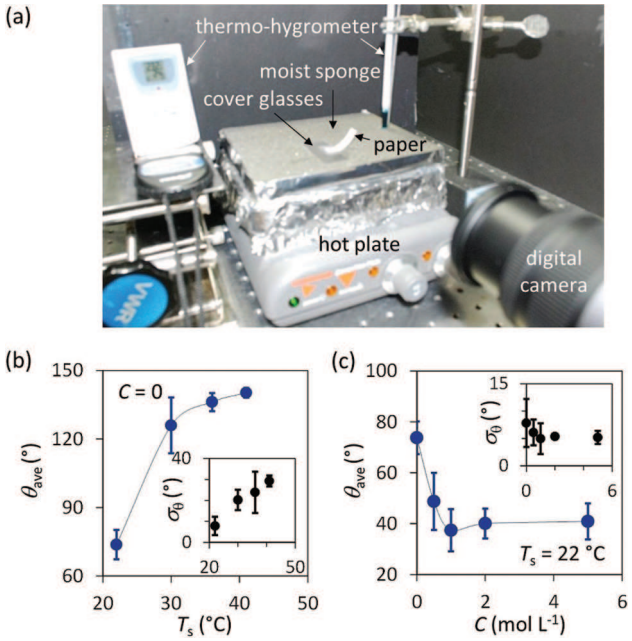


Fig. 7: (Color online) Sensitivity of paper to alterations in the substrate. (a) Photograph of the experimental setup used for the investigation of the effects of surface temperature $T_s$ and salt concentration $C$ on the shape of the paper cantilever (same dimension and configuration as those in fig. 2(a)). (b), (c): measured average bending angle $\theta_{ave}$ with a deviation $\sigma_\theta$ (inset) of the paper as a function of $T_s$ (at $C = 0$) and $C$ (at $T_s = 22\,^\circ$C), respectively. The error bars represent the standard deviation of at least three independent measurements.

The experimental setup shown in fig. 7(a) was used to investigate the effects of surface temperature and salinity. The temperature at the surface of a moist sponge was controlled by a temperature adjustable hot plate (Stirrer/Hot Plate, Corning) underneath the aluminum container. Four different surface temperatures were used: $T_s = [22.4\pm0.2]$, $[29.9\pm0.2]$, $[35.6\pm0.3]$, and $[40.6 \pm 0.5]\,^\circ$C at constant $H_\infty \approx 28\%$. The salt solutions were made up of NaCl dissolved in distilled water. In this study, four different salt concentrations $C$ in the range from 0 to 5 mol L$^{-1}$ were used. The bending responses of paper cantilevers (length = 25 mm, width = 10 mm) deposited on a moist sponge with different surface temperatures and concentrations were recorded and the results are summarized in fig. 7(b), (c).

The experimental realization of the paper-based actuators presented in fig. 4 was conducted on the surface of a moist sponge having a size of 540 mm × 420 mm and a thickness of 25 mm with ≈ 500 mL of pure water. A small piece (≈ 50 mm square) of the weighing paper was modified as illustrated in fig. 4(a), (d) and then gently placed on the moist surface. The resulting paper motion was recorded using a digital-camera system. Note that the time $t = 0$ in fig. 4 is the time when the paper rests freely on the substrate.

In the experiment shown in fig. 4(d), a thin layer of paraffin wax was applied to the selected regions of the weighing paper by painting with a crayon. Static water contact angle (WCA) measurements were performed by dispensing a droplet (≈ 10 $\mu$L) of distilled water on specimens, and the change in droplet size due to evaporation and/or penetration into the paper was examined and photographed with a digital camera. The results indicate that the wax-coated surface of the paper is hydrophobic with initial WCA of $[107\pm3]^\circ$ and effectively prevents the permeation of water (thus, moisture) into the porous paper. Note that the initial WCA of the virgin surface of the paper was $[59\pm2]^\circ$, which gradually decreased to near 0°.

REFERENCES


[1] Fratzl P. and Barth F. G., *Nature*, **462** (2009) 442.
[2] Mirfakhrai T., Madden J. D. W. and Baughman R. H., *Mater. Today*, **10**, issue No. 4 (2007) 30.
[3] Ma M. M., Guo L., Anderson D. G. and Langer R., *Science*, **339** (2013) 186.
[4] Dawson C., Vincent J. F. V. and Rocca A.-M., *Nature*, **390** (1997) 668.
[5] Elbaum R., Zaltzman L., Burgert I. and Fratzl P., *Science*, **316** (2007) 884.
[6] Reyssat E. and Mahadevan L., *J. R. Soc. Interface*, **6** (2009) 951.
[7] Lin H.-T., Leisk G. G. and Trimmer B., *Bioinspir. Biomim.*, **6** (2011) 026007.
[8] Chen X., Mahadevan L., Driks A. and Sahin O., *Nat. Nanotechnol.*, **9** (2014) 137.
[9] Alava M. and Niskanen K., *Rep. Prog. Phys.*, **69** (2006) 669.
[10] Kabla A. and Mahadevan L., *J. R. Soc. Interface*, **4** (2007) 99.
[11] Uesaka T., Moss C. and Nanri Y., *J. Pulp Pap. Sci.*, **18** (1992) J11.
[12] Rance H. F., *The Structure and Physical Properties of Paper* (Elsevier Scientific, Amsterdam) 1982.
[13] Kim J., Yun S. and Ounaies Z., *Macromolecules*, **39** (2006) 4202.
[14] Reyssat E. and Mahadevan L., *EPL*, **93** (2011) 54001.
[15] Douezan S., Wyart M., Brochard-Wyart F. and Cuvelier D., *Soft Matter*, **7** (2011) 1506.
[16] Machin J., *J. Exp. Biol.*, **53** (1970) 753.
[17] Ramsay J. A., Butler C. G. and Sang J. H., *J. Exp. Biol.*, **15** (1938) 255.
[18] Timoshenko S., *J. Opt. Soc. Am.*, **11** (1925) 233.
[19] Ramarao B. V., Massoquete A., Lavrykov S. and Ramaswamy S., *Drying Technol.*, **21** (2003) 2007.
[20] Larsson P., *Hygro- and hydroexpansion of paper*, PhD Thesis, KTH Royal Institute of Technology (2010).